

Article

Combining a Fatigue Model and an Incremental Capacity Analysis on a Commercial NMC/Graphite Cell under Constant Current Cycling with and without Calendar Aging

Tiphaine Plattard ^{1,2,*}, Nathalie Barnel ¹, Loïc Assaud ², Sylvain Franger ^{2,*} and Jean-Marc Duffault ²

¹ EDF R&D Les Renardières, 77250 Moret Loing et Orvanne, France; nathalie.barnel@edf.fr

² ICMMO-ERIEE, Université Paris-Sud, Université Paris-Saclay, CNRS UMR 8182, 91400 Orsay, France; loic.assaud@u-psud.fr (L.A.); jean-marc.duffault@u-psud.fr (J.-M.D.)

* Correspondence: tiphaine.plattard@edf.fr (T.P.); sylvain.franger@u-psud.fr (S.F.); Tel.: +33-160-736-059 (T.P.)

Received: 21 December 2018; Accepted: 13 March 2019; Published: 21 March 2019



Abstract: Reliable development of LIBs requires that they be correlated with accurate aging studies. The present project focuses on the implementation of a weighted ampere-hour throughput model, taking into account the operating parameters, and modulating the impact of an exchanged ampere-hour by the well-established three major stress factors: temperature, current intensity (rated), and state of charge (SoC). This model can drift with time due to repeated solicitation, so its parameters need to be updated by on-field measurements, in order to remain accurate. These on-field measurements are submitted to the so-called Incremental Capacity Analysis method (ICA), consisting in the analysis of dQ/dV as a function of V . It is a direct indicator of the state of health of the cell, as the experimental peaks are related to the active material chemical/structural evolution, such as phase transitions and recorded potential plateaus during charging/discharging. It is here applied to NMC/graphite based commercial cells. These peaks' evolution can be correlated with the here-defined Ah-kinetic and \sqrt{t} -kinetic aging, which are chemistry-dependent, and therefore, has to be adjusted to the different types of cells.

Keywords: lithium-ion; NMC; aging; ampere-hour throughput; incremental capacity analysis

1. Introduction

Rechargeable lithium-ion batteries (LIBs) appear to be the best system for energy storage in many applications, especially electric vehicles and stationary mass storage in the context of the energy transition. Any system employing Li-ion cells must be informed of the amount of energy that can be stored and the power that can be provided by the battery at any time. Therefore, reliable developments need to be correlated with accurate aging studies.

The aging of a battery leads mainly to loss of capacity, loss of power, and increase of internal resistance. The understanding of the underlying mechanisms is fundamental in order to provide an accurate and reliable aging prediction in the models. However, it is not always easy to build a strong model, since the battery cell consists of a complex system including interactions between several domains: mainly, physics, electrochemistry, and thermal sciences. Qualitative aging of the battery has been studied in all these fields, regarding electrolyte degradation, solid electrolyte interphase (SEI) formation, or mechanical deformations [1–4].

A LIB is expected to have a life span of more than 10 years. Therefore, the implemented model should predict the aging of a LIB in the long-term, and have a fast computation time.

In order to produce a quantitative aging estimation, cell degradation needs to be studied under various aging conditions, and models need to be strengthened with on-field measurements in order to generate predictions of energy storage capacity and power capability. Several generations of LIBs have been tested both at EDF Lab Les Renardières facility and Université Paris-Sud ICMMO Lab, using specific protocols and monitoring aging degradations.

Many different models have been developed so far to evaluate the electrochemical behavior of batteries:

- fundamental models or physical models;
- phenomenological models or empirical models; and
- mathematical models.

They are described in the following sections.

1.1. Fundamental Models

Physical models appreciate the aging of a battery by precisely describing the internal mechanisms, such as ion transport in the electrolyte or within the electrode active material, charge transfer at the electrode/electrolyte interface, thanks to partial differential equations, Fick's law, or the Butler–Volmer equation for example. Newman and Fuller have developed the porous electrode model [5], extended by Ramadass et al. to take into account the loss of capacity during each cycle [6]. An approximation of the lithium-ion concentration profile within the solid phase has been presented by Wang et al. [7] and by Subramanian et al. [8]. A simpler physical model has been introduced by Haran et al. that represents each electrode as a simple spherical particle [9], it has been extended to LIB by Ning et al. [10], and further studied by Delacourt and Safari [11].

The advantage of the porous electrode model's is that it takes into account almost all the physical processes taking place while battery is cycling, however solving it is time consuming and many required parameters cannot be verified. The simple spherical particle is easier to solve but does not encompass all the mechanisms. One has to remember that the computation time is crucial since the model has to be recomputed at every cycle. The influence of each separate aging parameter (temperature, state of charge, and rated current) on the model has, to our knowledge, never been developed.

1.2. Phenomenological Models

Despite physical models, the phenomenological models provide links between inputs and outputs of the system, without a comprehensive examination of the physical phenomena taking place. A simple structure is enough to solve the model. Instead of equations, this model consists of experimental and extrapolated curves. Experimental knowledge obtained with these models can circumvent an equational or theoretical problem.

Among these models designed for lithium-ion batteries, we find the fatigue models, like the one originally designed by Dudézert and Franger [12] and refined by Badey and Franger [13]. The model tends to modulate the impact of an exchanged ampere-hour by the conditions in which it is exchanged. Mathematical functions of the current, the state of charge, and the rated current are therefore established as weighting functions. Therefore, this model is natively able to decipher the contribution of each aging parameters: temperature, state of charge, and rated current. The second strength of this model is being able to distinguish the two contributions of aging to the cell: calendar aging proportional to the root square of time and cycling aging proportional to the total ampere-hours exchanged. Indeed, the aging of a battery occurs both when the battery is in use, corresponding to the cycling aging, and when it remains unused, corresponding to the calendar aging. The aging can be thus modeled by two different contributions: an active regime loss and a temporal one.

Previous attempts to do so include Baghdadi et al. [14], who suggested an exponentially decreasing capacity with time, or Bloom et al. [15], who proposed a model where the temperature follows an

Arrhenius law. Most of the authors use a root square dependency to describe the calendar loss of capacity [13–16]. Other authors suggest multiplying a degradation coefficient of the calendar aging to the cycling one. Badey's model includes the two most important features required in our case: decoupling between the calendar and cycling aging, thanks to a sum of two terms, and identification of each parameter's impact.

1.3. Mathematical Models

Mathematical models require a huge amount of data in order to find a link between inputs and outputs. They are based on numerical resolution, and use probabilistic or statistical methods. Generally speaking, they cannot extrapolate to a situation that was not given in the initial set of data. Given the ongoing increasing volume of data and their valorization, one can think these models will play an important role in the future. However, they do not embed any expertise. Furthermore, the error cannot be controlled.

The model chosen to establish our own aging model is based on the fatigue model of Badey. The functions have already been explained thermodynamically [17]. However, fatigue models drift with repeated solicitation, so that their parameters need to be regularly reevaluated. This is what the incremental capacity analysis (ICA) will allow.

In this contribution, we aim at investigating and establishing a link between the ICA and the loss of calendar and cycling capacity, as defined in our model. Our model would then be able to be reparametrized thanks to this metric computed on-field. In this paper, the evolution of the ICA peaks obtained for NMC/graphite cells are discussed to provide a comprehensive interpretation.

The first part of this paper focuses on the aging model implementation and experimental and model basics, whereas the second part deals with the integration of the incremental capacity analysis as a way to explain the degradation process in a quantitative manner.

2. Materials and Methods

In this piece of work, commercial NMC/graphite cells were considered. Due to confidentiality, the cell manufacturer cannot be named. The main technical characteristics of the cells are summarized in Table 1.

Table 1. NMC cell technical characteristics.

Cell	Capacity	Cut-Off Voltages	Charging Protocol
NMC/Graphite	64 Ah	4.2 V/3 V	CC-CV

The cells received were surveyed by weight and open-circuit voltage (OCV) measurements. Variations in OCV with temperature have also been measured.

NMC is very much considered nowadays because it enables very good cyclability as well as good capacity: 180–200 mAh/g. However, NMC suffers from noticeable manganese dissolution in the electrolyte.

All cells were tested with laboratory-made racks, enabling air ventilation. It is important to pay close attention to cell connections to the power channel, in order to minimize variability and achieve better consistency in tests results. All cells used in the tests were submitted to an initial check-up, also called the Reference Performance Test (RPT). Therefore, cells with close initial characteristics (capacity, weight) were selected to go through the aging tests, described by Delétang et al in [17] and in Table 2. The average OCV recorded at 30 °C is 3.60 V, which corresponds to a SOC of ~40%.

Table 2. Aging test matrix.

Cell Number	Temperature/°C	SOC	I Charge	I Discharge
1	T1 = 10	100%		
2	T1 = 23	100%		
3	T1 = 45	100%		
4	T1 = 55	100%		
5a	T1 = 45	15%	1C	1D
5b	T1 = 45	30%	1C	1D
5c	T1 = 45	50%	1C	1D
5d	T1 = 45	80%	1C	1D
6a	T1 = 45	50%	C/2	1D
6b	T1 = 45	50%	1C	D/2
7a	T1 = 23	50%	1C	1D
7b	T1 = 23	30%	1C	1D
8	T2 = 10	50%	1C	1D

The RPT procedure was performed at 23 °C and consists of the following steps; constant current phase charge at a regime of C/3, followed by a constant voltage phase at 4.2 V until the termination current C/20 was reached, then charge and discharge resistance pulses for 10 s at 1C current every 3.2 Ah discharged until the cutoff voltage is reached (3.0 V), the complete recharge at C/3 CC-CV, and then complete CC discharge at C/2 until the cutoff voltage is reached. This last discharge provides the remaining capacity. The detection of capacity fading therefore requires columbic counting of a full charge/discharge cycle. The cell is finally charged to 50% nominal SOC in order to achieve an electrochemical impedance spectroscopy measurement. This latter is done at SOC 50%. The measurements were performed using the battery testing bench VMP Biologic multichannel potentiostat.

Capacity remaining was thus measured at C/2 discharge regimes. The datasheet featured a 64 Ah capacity. The average value was 62.93 Ah, and the capacity measured was quite consistent among all cells (the median value being 62.92 Ah, the standard variation being 0.17 (0.27%), there is little cell-to-cell variation), demonstrating the cell quality in performance. This cell-to-cell variation of 0.27% is satisfying when compared to literature [18].

The resistance pulses allowed computing the polarization resistance of the cell. It was calculated from the difference in voltage drops using Ohm's law: $\Delta V = I R$.

A series of tests were launched so that cells undergo unitary aging tests.

The aging parameters were temperature (in °C), rated-current C-rate (abusively written I in A/Ah), and the state of charge of the battery (SOC in %). Cycling aging was performed at an approximation of the adequate value of SOC with a depth of discharge (DOD) of 10%, so that the aging of the cell can be considered as due to the defined SOC. The cycling process was the following: the cell was first charged to 100% SOC at C/3 in CC-CV mode, it is then discharged to the targeted SOC subtracted by 5% at a rate of C/3. Then a rest of 1 h is imposed before the ulterior cycles start.

The values of the parameters have been chosen in order to be aligned with the real applications in use. Especially, temperature does not exceed 55 °C and is never lower than 10 °C. The test facility is air conditioned to maintain a stable temperature. Due to difference in charge and discharge efficiency, the SOC, around which the cell is being cycled, tends to decrease with cycling. Therefore, every 100 cycles at 10% DOD, the re-SOC is imposed to the cell. It is a common test procedure, as described by Delacourt et al. [19]. Approximately every 3000 cycles at 10% DOD the cell was subjected to a RPT to assess changes in performance.

Impedance measurements associated with the RPT was performed in galvanostatic mode as recommended for LIB in which the voltage changes during testing. The current amplitude was set to 1 A, which shows a good signal-to-noise ratio and stays in the linear region. The frequency swept between 10 kHz to 10 mHz. All measurements were carried out at 23 °C.

3. Results

3.1. Cycling Aging

The usual test procedure, like the one mentioned in the European Standard CE NF 50,272 which specifies safety requirements for secondary batteries and battery installations, defines the end-of-life of a battery when it cannot deliver more than 80% of its initial capacity under a specific test protocol. At this time, the cells were at ~10/12%-capacity loss, constituting a huge volume of recorded data. Only some selected results are presented here.

Figure 1 presents the evolution of capacity over the 45 °C cycling for the different SOC. As explained in the above section, the discharge rate was C/2. It has to be noted that the higher the SOC, the higher the fade rate, except for SOC 15% that features a higher degradation rate than SOC 30%.

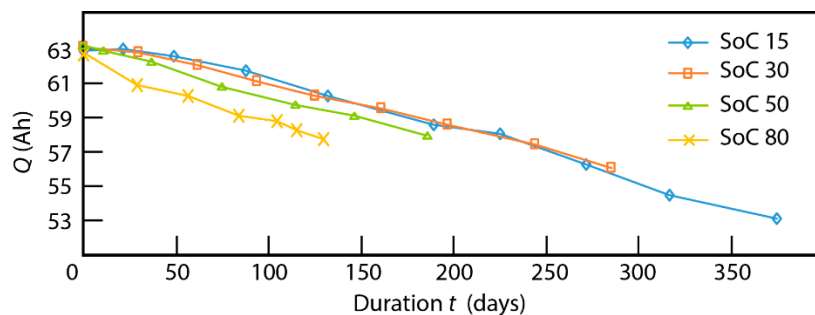


Figure 1. Evolution of the remaining cell capacity with respect of time, for aging at 45 °C at different state of charge (SOC).

The data were subsequently computed to apply the fatigue model [11,12], of which, the main capacity evolution equation is mentioned below.

$$\Delta Q = K^{cyc} f_1(T) f_2(I) f_3(SOC) \cdot Ah + K^{cal} g_1(T) g_2(I) g_3(SOC) \cdot \sqrt{t}$$

where K^{cyc} and K^{cal} are two constant coefficients specific to the cell considered. The loss of capacity is the sum of two terms: the first one is called the cycling aging and the second one is called the calendar aging. This separation is more and more specifically addressed in the literature [20,21].

For each data set, the linear regression of the function $\Delta Q / (\sqrt{t})$ with respect to $(CT \text{ (Ah)}) / (\sqrt{t})$ provides two coefficients, as seen on Figure 2, A,B defined as follows

$$\begin{aligned} A &= K^{cyc} f_1(T) f_2(I) f_3(SOC), \\ B &= K^{cal} g_1(T) g_2(I) g_3(SOC), \end{aligned}$$

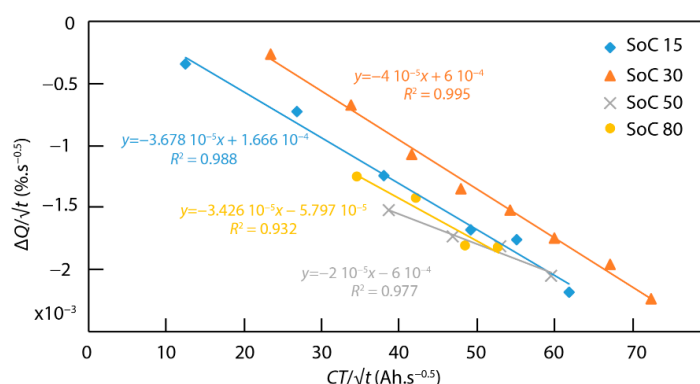


Figure 2. $\Delta Q (\%) / \sqrt{t}$ as a function of $CT \text{ (Ah)} / \sqrt{t}$ ($CT \text{ (Ah)}$ stands for the total exchanged ampere-hours).

These two coefficients allow to extract the values of the weighted functions f_i and g_i , and to decipher the capacity fade due to calendar aging and the loss due to cycling aging [17]. The cycling aging of an aging test is equal to $A \cdot Ah$ and the calendar aging is equal to $B \cdot \sqrt{t}$. Therefore the cycling aging is proportional to the number of ampere-hours exchanged and the calendar aging is proportional to the square root of time. This latter square root of time dependency is, however, discussed by Dubarry [22], who compared it with a $t^{3/4}$ and a t dependency. The \sqrt{t} obtained the best fit, so that the authors used it in the end.

3.2. Incremental Capacity Analysis

Figure 3a displays the evolution of the IC curves with time for cell aged at 45 °C at ~50% SOC at 1C/1D (denoted as (45°, SOC 50, 1C/1D)). In the same manner, Figure 3b stands for (45°, SOC 30, 1C/1D), Figure 3c stands for (45°, SOC 15, 1C/1D), and Figure 3d stands for (45°, SOC 80, 1C/1D). It exhibits two different peaks: the highest peak (maximum at ~3.6 V) and the second peak (maximum at ~3.4 V), which is coherent with what is observed by Berecibar et al. [23]. The highest peak has a symmetrical shape. Qualitatively, the most striking feature is that the intensity of the highest peak and of the second peak decreased for different states of health, which is coherent with the few NMC-based ICA study [21,23,24]. The average voltage of the maximum intensity of the highest peak is shown in Table 3. The average value was stable and the standard deviation was almost zero. This voltage remained stable with time (aging), and the highest peak is simply denoted as “3.5 V-peak” in the following sections. It seems that the curve remained in the same shape around the extrema of voltage values, indicating that the kinetics of the cell reaction has not been affected. As shown in Table 3, the average voltage of the maximum intensity was not as stable as the highest one. The standard deviation was also higher.

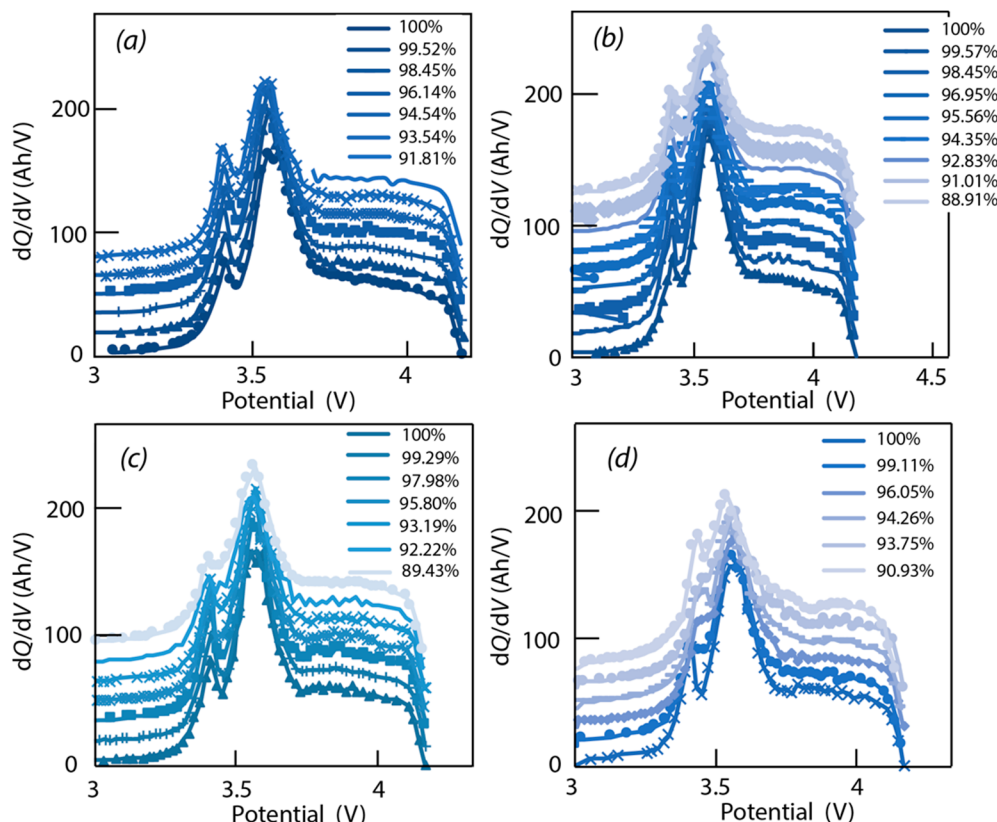


Figure 3. IC curves obtained for (a) (45°, SOC 50, 1C/1D), (b) (45°, SOC 30, 1C/1D), (c) (45°, SOC 15, 1C/1D), and (d) (45°, SOC 80, 1C/1D) at different states of health. A vertical offset was added for the sake of clarity: the curves have a 15 Ah/V-offset each.

Table 3. Average value of voltage and standard deviation for 3.5 V and 3.4 V peak maxima.

	Average Voltage of the Maximum of the 3.5 V Peak	Standard Deviation 3.5 V	Average Voltage of the Maximum of the 3.4 V Peak	Standard Deviation 3.4 V
(45 °C, 15%, 1C/1D)	3.57	0.01	3.42	0.03
(45 °C, 30%, 1C/1D)	3.56	0.01	3.41	0.01
(45 °C, 50%, 1C/1D)	3.55	0.01	3.43	0.04
(45 °C, 80%, 1C/1D)	3.56	0.01	3.43	0.02
(23 °C, 30%, 1C/1D)	3.57	0.00	3.41	0.00
(23 °C, 50%, 1C/1D)	3.55	0.01	3.42	0.03
(10 °C, 50%, 1C/1D)	3.56	0.01	3.43	0.01

Changing the temperature, the tests (23° , SOC 50, 1C/1D; 23° , SOC 30, 1C/1D) feature similar behaviors in IC curves, as shown in Figure 4.

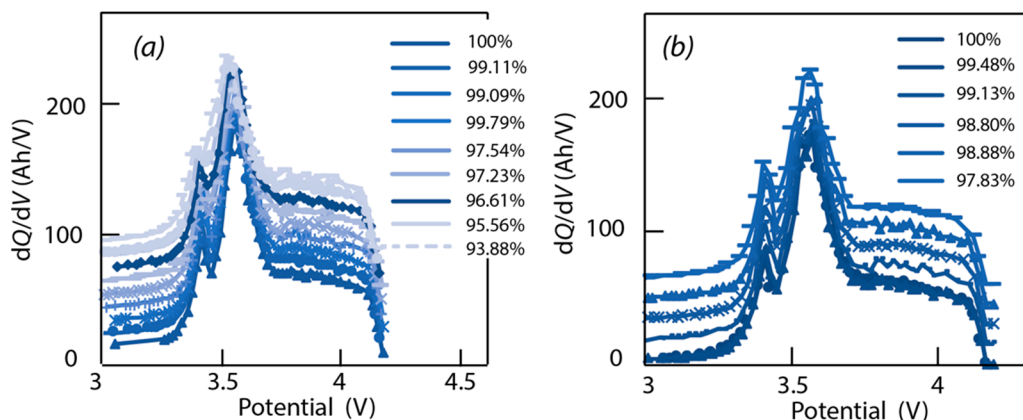


Figure 4. IC curves obtained for (a) 23° , SOC 50, 1C/1D and (b) 23° , SOC 30, 1C/1D. A vertical offset was added for the sake of clarity: the curves have a 10 Ah/V-offset and 15 Ah/V-offset.

The peak area has been defined for the 3.5 V peak, as the area under the curve comprised between the peak's voltage value and is symmetrical, as described on Figure 5. It corresponds to the capacity involved in the related reaction happening in between the borders. For the 3.4 V peak, it is defined as the area under the curve comprised between the peak voltage value and the cutoff voltage of 3.0 V.

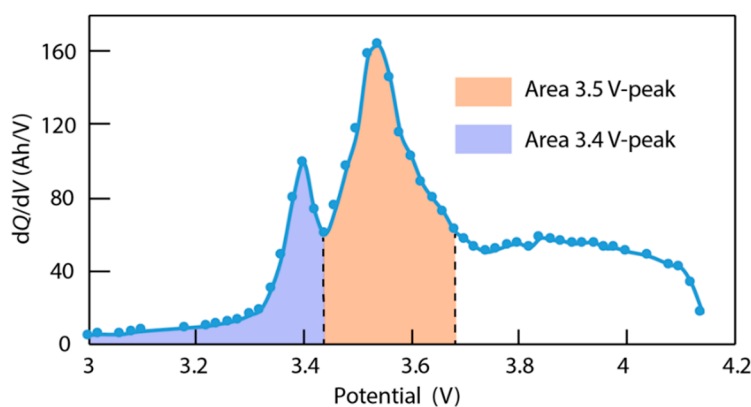


Figure 5. Incremental capacity analysis (ICA) versus voltage for one cell at the initial state, obtained for $dV = 20$ mV. AP-3.5 V is the area of the peak at 3.5 V and AP-3.4 V is the area of the peak at 3.4 V.

It can be observed that the 3.5 V peak area is linearly proportional to the total loss of capacity due to cell aging, which is coherent with [25,26].

The correlation coefficient of that left curve (Figure 6) is quite high (0.97), the other one is weaker. Others are also strongly correlated as shown in Table 4.

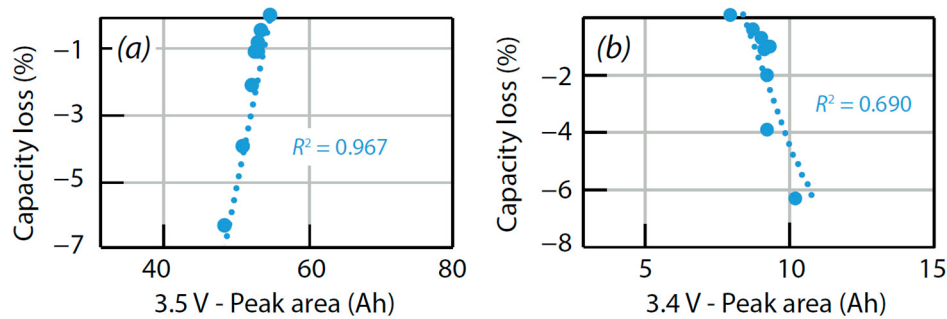


Figure 6. Capacity loss (%) as a function of peak area (3.5 V) (Ah) for cell (23°C , SOC 30, 1C/1D) ((a) is for the 3.5 V peak and (b) is for the 3.4 V peak).

Table 4. Correlation coefficient of highest peak with the total loss of capacity for different tests.

Test Description	Correlation Coefficient HP-3.5 V//Loss Capacity	Correlation Coefficient HP-3.4 V//Loss Capacity
(45 °C, 15%, 1C/1D)	0.97	0.93
(45 °C, 30%, 1C/1D)	0.97	0.91
(45 °C, 50%, 1C/1D)	0.95	0.78
(45 °C, 80%, 1C/1D)	0.90	0.73
(23 °C, 30%, 1C/1D)	0.96	0.69
(23 °C, 50%, 1C/1D)	0.98	0.92
(10 °C, 50%, 1C/1D)	0.80	0.63

These first cycling tests show that the highest peak (3.5 V) seems to be strongly correlated with the total loss of capacity. In order to decipher between the calendar contribution ($B\sqrt{t}$) and the cycling contribution ($A\text{Ah}$) of our aging model, we were interested in determining if the area of the peak (labeled A) could be correlated to the Ah-exchanged or to the root square of t , as suggested by Cabelguen [18] and Riviere [27]. The correlation coefficient is shown in Table 5.

Table 5. Correlation coefficient of highest peak area with Ah and \sqrt{t} for different tests.

Test	Correlation Coefficient Peak 3.5 V//Ah	Correlation Coefficient Peak 3.4 V// \sqrt{t}
(45 °C, 15%, 1C/1D)	0.97	0.98
(45 °C, 30%, 1C/1D)	0.98	0.71
(45 °C, 50%, 1C/1D)	0.94	0.76
(45 °C, 80%, 1C/1D)	0.82	0.32
(23 °C, 30%, 1C/1D)	0.81	0.97
(23 °C, 50%, 1C/1D)	0.98	0.93
(10 °C, 50%, 1C/1D)	0.88	0.53

With all the correlation coefficients above 0.81 for 3.5 V, in terms of modeling, it seems to be safe to consider the highest peak to be correlated to the Ah-exchanged. The second peak (3.4 V peak) seems to be correlated to the square root of time, although some quite low coefficients were determined.

The Ah-results summarized in Table 6 were not convincing enough as they do not show a clear trend about the 3.4 V peak, as discussed earlier. This is probably due to the difficulty in removing the cycling part in the calendar part with this criterion. Furthermore, considering only calendar aging tests at four different temperatures—10 °C, 23 °C, 45 °C, and 55 °C—the correlation between the area of the peak and the root square of the time was almost ideal, except for (55 °C, 100%, CAL). This confirms that cycling aging has an impact in the calendar aging contribution of the global capacity loss.

Table 6. Correlation coefficient of 3.4 V peak with Ah and \sqrt{t} for different tests.

Test	Correlation Coefficient Peak 3.4 V//Ah	Correlation Coefficient Peak 3.4 V// \sqrt{t}
(45 °C, 15%, 1C/1D)	0.96	0.98
(45 °C, 30%, 1C/1D)	0.88	0.71
(45 °C, 50%, 1C/1D)	0.84	0.76
(45 °C, 80%, 1C/1D)	0.26	0.32
(23 °C, 30%, 1C/1D)	0.20	0.97
(23 °C, 50%, 1C/1D)	0.86	0.93
(10 °C, 50%, 1C/1D)	0.37	0.53
(55 °C, 100%, CAL)	—	0.56
(45 °C, 100%, CAL)	—	0.85
(10 °C, 100%, CAL)	—	0.99
(23 °C, 100%, CAL)	—	0.94

The last strategy was to seek if the area AP of that 3.4 V peak could follow the same kinetic as the loss of capacity, and then evaluate the predominant part of aging that affects that peak. We have thus computed the following equation, searching for alpha and beta coefficients.

$$\frac{\Delta AP}{\sqrt{t}} = \text{alpha} \cdot \frac{Ah}{\sqrt{t}} + \text{beta}$$

Table 7 shows the corresponding correlation coefficients.

Table 7. Correlation coefficient of 3.4 V peak with ($\text{alpha} * \text{Ah}/\sqrt{t} + \text{beta}$) for different tests.

Test	Correlation Coefficient Peak 3.4 V//Alpha and Ah/ \sqrt{t} + Beta
(45 °C, 15%, 1C/1D)	0.70
(45 °C, 30%, 1C/1D)	0.92
(45 °C, 50%, 1C/1D)	0.97
(45 °C, 80%, 1C/1D)	0.18
(23 °C, 30%, 1C/1D)	0.78
(23 °C, 50%, 1C/1D)	0.66
(10 °C, 50%, 1C/1D)	0.26

The correlation coefficients were quite satisfying for three tests: (45 °C, 30%, 1C/1D), (45 °C, 50%, 1C/1D), and (23 °C, 30%, 1C/1D). The coefficients alpha and beta are not significant enough to be compared, as they are $\sim 10^{-6}$. This seems to be a promising path in order to better distinguish the different processes of aging taking place in the cell, to be further studied.

In terms of the model, we proposed assigning the Ah-kinetic of our aging model to the area of the 3.5 V peak and the Ah-kinetic and \sqrt{t} -kinetic aging to the area of the 3.4 V peak.

4. Discussion

4.1. Background on Aging Mechanisms

Aging can generally be due to three main causes:

- Loss of lithium inventory (LLI) is caused by the consumption of Li cations by parasitic reactions of which the major remains the well-known SEI growth at the negative electrode. Therefore, less and less lithium ions are available to shuffle back and forth in the electrodes, captured in the electrode bulk or inside the electrolyte aggregates. The reactions lead to by-products released in the electrolyte, which can further cause side reactions [28,29]. This aging cause can often explain the first stages of the aging. The impact on the potential of LLI, as explained by Bloom et al.

in [30], is that as the side reactions proceed, the lower potential regions of the NE would be removed, and thus, charging the cell would incompletely lithiate the NE. Compared to its initial state, at the end of charge, the NE is now at a higher potential. To maintain the upper limit value, there would be a shift to compensate at the positive electrode to higher potentials. However, in the graphite, the end of charge is a plateau and the potential of the PE will not very much.

- Loss of active material (LAM): insulation of active material with loss of contacts with the conductive matrix, dissolution of transition metal in the electrolyte, structural changes in the crystalline structure of anode, and cathode active materials due to repeated insertions/disinsertions of ions. LAM appearing at the negative electrode only (LAM NE) and LAM appearing at the positive electrode only (LAM PE) have to be differentiated. Dubarry et al. [28] even separate LAM on delithiated and LAM on lithiated electrodes. The impact of LAM on the potential of PE and NE is well explained in Figure 6 of ref. [31] and by Matadi [16] and Dubarry [32,33].
- Conductivity loss (CL): increasing of the faradic resistance due to mass transport slowdown or ionic conduction in the bulk of the electrode and increasing of the ohmic resistance due to contacts degradations in the electrodes or in the electrolyte conduction. CL only affects the cell voltage, not the capacity.

These mechanisms are schematically separated here, but they are coupled during the aging process. Dubarry et al. used a very suitable analogy with a water clock [24], composed of two connected bulbs filled with a given amount of liquid. LAM affects the size of the bulb and LLI affects the amount of available liquid, if there was a leak in the water clock. They have also constructed a comprehensive toolbox “alawa” to simulate these phenomena [31]; it is used in Section 4.4.

4.2. Background on ICA

The Incremental Capacity Analysis (ICA), meaning the analysis of dQ/dV as a function of V (dQ corresponds to the change in capacity that happens in the gap dV) is a direct indicator of the state of the cell. Differential Voltage Analysis (DVA), which analyses dV/dQ as a function of Q , is not appropriate for our study since the reference (x -axis) varies when capacity fades [26,31]. dV/dQ highlights single phase regions whereas dQ/dV curve represents the phase transformations [25,26,34,35]. The peaks represent the electrochemical mechanisms occurring in the cell. They are mainly related to the chemistry of the cell [23–33].

ICA is more beneficial when the cell is at equilibrium. Discharge regimes should therefore be small, approximately C/20 or C/25. However, these very low rates require too much time in real application (approximately 50 h to complete a charge and discharge cycle). As proven by Li [26], one can take benefit from this technique until 1C regime. In the above 1C regime, the results are erratic and not exploitable [32].

The evolution of the voltage of the cell during a discharge of 100% DOD shows the variations of voltage (that indicates what reaction is taking place) as a function of displaced charges (meaning capacity, which shows the extent of that reaction), as shown in Figure 7. Two clear voltage plateaus can be identified from that curve, approximately 3.4 V and 3.6 V. A voltage plateau on a full cell means both electrodes are experiencing phase transformations (there is coexistence of two distinct phases on each electrode) [27]. As a phase depends on the quantity of lithium ions inserted in the electrode, the information about the battery aging mechanism is contained in the shift of these plateaus. The dQ/dV analysis estimates the capacity displaced in each incremental change of voltage in the reaction. However, it does not only provide pieces of information on electrochemical reactions occurring inside the cell (through voltage plateau for example) but its evolution with time reveal how these reactions are affected by aging.

The principle of the ICA is therefore clear: the peaks obtained at different aging states RPTs provide an aging signature and enable identification of the degradation modes (LAM PE, LAM NE, LLI, and CL). A peak is characterized by a voltage position and its area (linked to its height also called intensity, which is deeply studied by Berecibar et al. [23]).

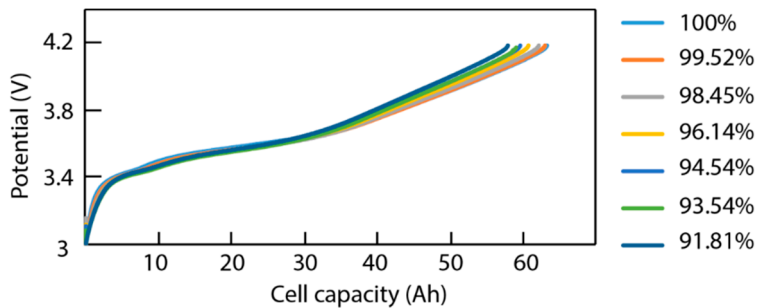


Figure 7. Evolution of the discharge curve of a cell with aging during a discharge at C/2 at 23 °C. Curves are shown according to their State of Health (SOH).

The final goal of using this metric is to be able to update the first fatigue model. Therefore, the correlation made previously between the peak and the calendar and cycling aging processes will be used in a numerical way. Having that correlation link, a discharge profile of the cell will lead to the updated real values of the weighted functions (and no more the predicted values), leading to the refinement of our model.

4.3. Data Analysis of ICA

The C/2 discharge data and very fast acquisition rate require mathematical filtering, to minimize the noise and enlighten the peaks. This filtering was done with Microsoft Excel, considering a fixed ΔV of 20 mV for discharge data (which is consistent with Bloom et al. [35,36] and Li et al. [37]). dQ then appears to be the exchanged charges during this given voltage step ΔV . For charge-related IC data, the ΔV depends on the rate of the charge so that the peaks can be observed and compared: 20 mV for 0.04 C, 10 mV for 0.2 C, and 2 mV for 0.33C. There is proportionality between these two values as shown in Figure 8.

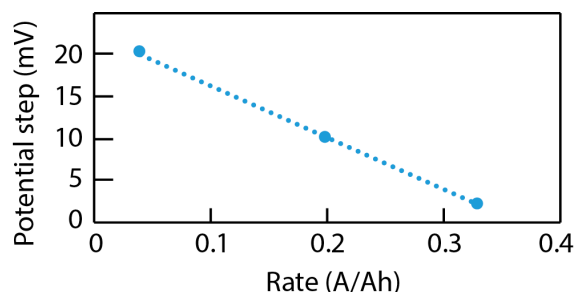


Figure 8. Voltage step chosen for charge ICA analysis as a function of the charge rate.

A plot of dQ/dV versus voltage for a cell at $t = 0$ during discharge is given in Figure 5. It contains primarily two peaks that can be assigned thanks to additional information, found in the literature. The first statement that can be made is that these two peaks correspond to two different electrochemical reactions taking place during discharge inside the whole cell (both anode and cathode). These peaks are strongly chemistry-dependent as mentioned in the literature [23,25,26].

Based on the literature, starting from the highest potential where the NMC electrode forms a solid solution, during discharge, the voltage of the cell decreases consistently from 4.2 V to 3.75 V (vs Li^+/Li), filling the NMC cathode of lithium ions [18]. In this stage, the graphite electrode content transfers from LiC_6 to LiC_{12} and then from LiC_{12} to LiC_{18} [18]. From the ripples in the IC curve of Figure 5, ~3.75 V can be due to the transition phase LiC_6 to LiC_{12} . This transition phase lasts much longer than the others in the graphite (it is kinetically slower) [34]. As no hysteresis between lithiation and delithiation in this phase was observed, this should be reversible and thus, not strongly affected by aging.

Then, the lithium intercalation inside the crystalline structure leads to a phase transformation of NMC at 3.75 V (vs. Li⁺/Li) [18]. Convolution of this reaction vs. the graphite negative electrode implies a decrease of 0.122 V (vs. Li⁺/Li) in the cell voltage, as the graphite transits from LiC₁₂ to LiC₁₈ (stage 2 transformation). This explains the observed peak at ~3.6V (3.75 V–0.122 V ≈ 3.6 V). The additional difference can be explained by additives in the electrolyte. This is the only NMC-based reaction, as confirmed by Li et al. [26].

The remaining reactions happening inside the cell are graphite-based. From LiC₁₈ to LiC₂₄, and even to LiC₃₆, the graphite potential (vs. Li⁺/Li) increases drastically up to 0.6 V. At this step, the PE is on a voltage plateau. Therefore, since PE potential is not changing, but the NE potential is, a new peak will appear. This could explain the second peak observed at 3.4 V.

LLI and LAM NE could be the aging cause for the 3.4 V-peak evolution, as this peak is graphite-related. It is well-known that LLI, leading mainly to SEI formation, occurs primarily at the negative electrode. Indeed, LLI induces a potential shift of the NE curve of $V = f(SOC)$ towards higher SOC (see Figure 7 of [31]). The last graphite reaction (LiC₁₈ to LiC₂₄ and to LiC₃₆, stage 4–5 transformation), that is involved in the 3.5 V-peak, will be progressively convoluted with a flatter PE-curve. Thus the convolution will lead to a thinner and more intense peak.

The 3.5 V-peak corresponds both to the PE reaction and the NE stage 2 transformation. With LLI, the NE curve ($V = f(SOC)$) will be shifted towards higher SOC relative to the PE. Therefore, the stage 2 transformation of NE will be initiated at higher SOC and prior to the start of the PE-reaction. Thus, less of the capacity involved in the stage 2 will convolute with the PE and the peak area will go down. One could suppose that LAM PE could be responsible as well. Indeed, as SEI grows, there is production of species resulting from the electrolyte decomposition that might accumulate on the active grain surface, which may cause isolation of the grains inside the electrode matrix. LLI would therefore result in LAM PE. This would explain the difficulty to separate both modes of aging based on the 3.4 V peak's evolution. In any case, it is well-established that the cycling aging affects more the cathode electrode (NMC) [12]. Therefore, the fact that the area under the 3.5 V peak appears to be proportional to the number of exchanged-ampere hours seems legitimate. This hypothesis needs to be confirmed.

However, because the aging has reached less than 10% of capacity loss, the predominant mode of degradation seems to be LLI. This could be confirmed in the fact that in [31], the authors attributed to LAM PE an exponential evolution and to LLI a linear evolution (with capacity loss): at the beginning, the exponential is hardly differentiable from the straight linear.

4.4. Verification of Assumptions Based on 'Alawa' Tool

Different degradation of scenarios has been simulated on the 'alawa' toolbox developed by Dubarry et al. [31]. The data used to simulate our full cell come from the software (Graphite and NMC electrode data), so it was compulsory to adjust the Loading Ratio and the Offset to fit the IC curve obtained as close as possible to our own IC curve. Figure 9 shows the resulting IC curves obtained for a G//NMC cell with LR = 1.2, OFS = -5, resistance = 1, and a discharge rate of C/25.

LAM PE corresponds to LAMdePE (delithiated state), as LAM occurring on the lithiated state is equivalent to LAMdePE plus some LLI (same for LAM NE).

These simulations show the following tendencies.

- LLI increases the 3.4 V peak intensity, and reduces the 3.5 V peak intensity. It confirms that less and less lithium is involved in NE stage 2-reaction through cycling. The remainder of the capacity that is not engaged in that stage 2-reaction remains available for the other reactions, thus the growing and earlier start of the 3.4 V peak.
- LAM PE reduces the 3.4 V peak intensity, until it disappears, and moves the 3.5 V peak to lower voltages (slightly) while decreasing its intensity slightly.
- LAM NE decreases slightly the 3.4 V peak and increases slightly the 3.5 V peak intensity.

Therefore, what we observed on the 3.5 V peak of our own cell seems indeed to be mostly due to LLI. The intensity evolution of the 3.4 V peak seems indeed to be a mix of LLI (that increases its intensity) and LAM NE (that reduces its intensity). The 3.4 V peak area is shown to be slightly increasing (Figure 6b). It is however difficult to decipher between LLI and LAM NE which one is dominating, since the ‘alawa’ toolbox is not designed to take into account the temperature and precise SOC impact.

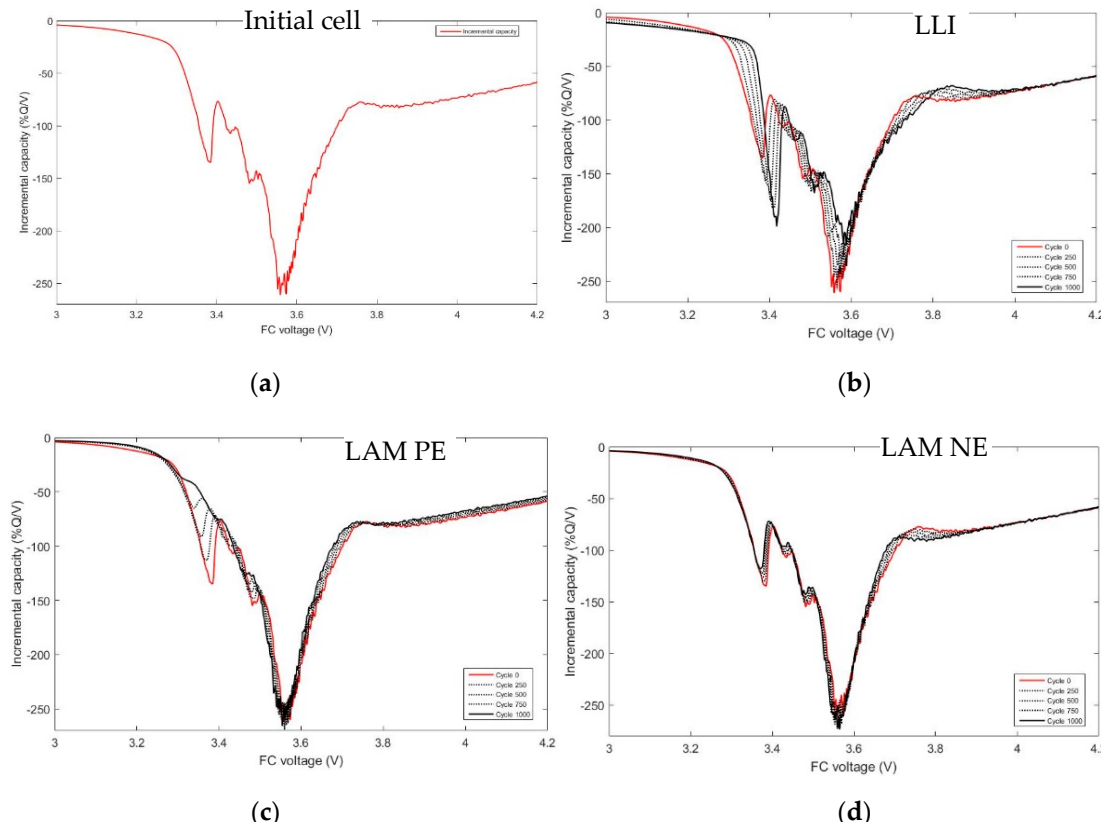


Figure 9. IC curves obtained from the ‘alawa’ toolbox: (a) Initial cell, (b) lithium inventory (LLI), (c) LAM PE, and (d) LAM NE. The red curve is the initial curve, and the other curves show the tendency of evolution every 250 cycles.

4.5. Connection between ICA and the Fatigue Model

The question arisen is how to combine the ICA observations and the fatigue model explained previously in Section 3.1.

The preliminary analysis of all the unitary aging tests leads to six weighting functions, and so six graphs (see the previously published graphs by Deletang et al. [17]). Being given a solicitation made of time steps, a rate, a temperature, and a SOC at each time step, the fatigue model will provide the infinitesimal (between two time steps) loss of cycling capacity ($A.Ah$), called $\delta_{f[i]}$, and the infinitesimal loss of calendar capacity ($B.\sqrt{t}$), called $\delta_{g[i]}$. With these two values, we can compute the value of the predicted remaining capacity at each time step. This is the direct pathway.

However, with on-field measurements, the value of the real capacity can be different from what has been predicted. So it is all about taking the reverse pathway: from the information of the on-field measurement, we extract the Incremental Capacity data and we update the $\delta_{f[i]}$ and $\delta_{g[i]}$ from which we then extract the weighted functions and, finally, we recompute the prediction with the updated weighting functions. To our knowledge, this has never been done before. Simulations from the developed software will be further published.

5. Conclusions

In this paper, we suggested a review to summarize the different aging models used for LIBs, and we presented the fatigue model used. Then we presented some results coming from an aging test campaign and suggested a link between an observable value (IC peak area), related to the discharge curve of a Li-ion cell, and the cycling and calendar capacity loss, defined in our fatigue model.

We observed two IC peaks for the studied NMC-based cell. One seems to be correlated to the number of exchanged ampere-hours, and thus could be correlated to what was defined as the “cycling aging” in our model. The other one is not clearly correlated to the root square of time, even if it is observed when considering cells aged only in calendar pattern (no exchanged ampere-hour). The difficulty in assigning a trend in the evolution of that peak would be due to the fact that calendar aging is also appearing during cycling. The alawa toolbox has been used to verify some assumptions.

The implementation of that result on another chemistry where the peaks’ position will change will be further studied.

As the IC peak degradation shown in the data is related to the first 10% of aging, the correlation needs to be verified for further degradation, where LLI is not the main degradation mechanism any longer [38–40]. Continuation of aging will clarify the explanation regarding LLI and LAM in order to further explain the loss of capacity.

Author Contributions: T.P., N.B., L.A. and S.F. developed the theoretical formalism, performed the analytic calculations. T.P. and N.B. performed the numerical simulations. T.P., L.A. and S.F. designed and performed the experiments. J.D. assisted with electrochemical analysis. T.P. wrote the manuscript in consultation with L.A., S.F. and N.B.

Funding: This research was funded by EDF R&D, Université Paris Sud/Université Paris Saclay ICMMO, and ANRT Agence Nationale de la Recherche et de la Technologie of France.

Acknowledgments: The authors gratefully acknowledge facilities provided by the EDF Lab Les Renardières, and ICMMO lab. The authors gratefully thank the Hawaii Natura Energy Institute for the disposal of the alawa toolbox.

Conflicts of Interest: The authors declare no conflicts of interest.

References

1. Vetter, J.; Novak, P.; Wagner, M.R.; Veit, C.; Moller, K.C.; Besenhard, J.O.; Winter, M.; Wohlfahrt-Mehrens, M.; Vogler, C.; Hammouche, A. Ageing mechanisms in lithium-ion batteries. *J. Power Sources* **2005**, *147*, 269–281. [[CrossRef](#)]
2. Broussely, M.; Biensan, P.; Bonhomme, F.; Blanchard, P.; Herreyre, S.; Nechev, K.; Staniewicz, R.J. Main aging mechanisms in Li ion batteries. *J. Power Sources* **2005**, *146*, 90–96. [[CrossRef](#)]
3. Grolleau, S.; Delaille, A.; Gualous, H.; Gyan, P.; Revel, R.; Bernard, J.; Redondo-Iglesias, E.; Peter, J. Calendar aging of commercial graphite/LiFePO₄ cell—Predicting capacity fade under time dependent storage conditions. *J. Power Sources* **2014**, *255*, 450–458. [[CrossRef](#)]
4. Novak, P.; Joho, F.; Lanz, M.; Rykart, B.; Panitz, J.-C.; Alliata, D.; Kötz, R.; Haas, O. The complex electrochemistry of graphite electrodes in lithium-ion batteries. *J. Power Sources* **2001**, *97–98*, 39–46. [[CrossRef](#)]
5. Fuller, T.F.; Doyle, M.; Newman, J. Simulation and Optimization of the Dual Lithium Ion Insertion Cell. *J. Electrochem. Soc.* **1994**, *141*, 1–10. [[CrossRef](#)]
6. Ramadass, P.; Haran, B.; White, R.; Popov, B.N. Development of First Principles Capacity Fade Model for Li-Ion Cells. *J. Electrochem. Soc.* **2004**, *151*, A196–A203. [[CrossRef](#)]
7. Wang, C.Y.; Gu, W.B.; Liaw, B.Y. Micro-Macroscopic Coupled Modeling of Batteries and Fuel Cells I. Model Development. *J. Electrochem. Soc.* **1998**, *145*, A3407–A3417. [[CrossRef](#)]
8. Subramanian, V.R.; Tapriyal, D.; White, R. A Boundary Condition for Porous Electrodes. *Electrochim. Solid State Lett.* **2004**, *9*, A259–A263. [[CrossRef](#)]
9. Haran, B.S.; Popov, B.N.; White, R. Determination of a hydrogen diffusion coefficient in metal hybrids by impedance spectroscopy. *J. Power Sources* **1998**, *75*, A56–A63. [[CrossRef](#)]
10. Ning, G.; Popov, B.N. Cycle life modeling of lithium-ion batteries. *J. Electrochem. Soc.* **2004**, *151*, A1584–A1591. [[CrossRef](#)]

11. Delacourt, C.; Safari, M. Life Simulation of a Graphite/LiFePO₄ Cell under Cycling and Storage. *J. Electrochem. Soc.* **2012**, *159*, 1283–1291. [[CrossRef](#)]
12. Dudézert, C.; Reynier, Y.; Duffault, J.-M.; Franger, S. Fatigue damage approach applied to Li-ion batteries ageing characterization. *Mater. Sci. Eng. B* **2016**, *213*, 177–189. [[CrossRef](#)]
13. Badey, Q. Etude des Mécanismes et Modélisation du Vieillissement des Batteries Lithium-ion Dans le Cadre d'un Usage Automobile. Ph.D. Thesis, Université Paris Sud, Orsay, France, 2012.
14. Baghdadi, I.; Briat, O.; Delétage, J.; Gyan, P.; Vinassa, J. Chemical rate phenomenon approach applied to lithium battery capacity fade estimation. *Microelectron. Reliabil.* **2016**, *64*, 134–139. [[CrossRef](#)]
15. Cole, B.; Sohn, J.J.; Bloom, I.; Jones, S.A.; Polzin, E.G. An accelerated calendar and cycle life study of li-ion cells. *J. Power Sources* **2001**, *101*, 238–247. [[CrossRef](#)]
16. Matadi Pilipili, B. Etude des Mécanismes de Vieillissement des Batteries Li-ion en Cyclage à Basse Température et en Stockage à Haute Température: Compréhension des Origines et Modélisation du Vieillissement. Ph.D. Thesis, Université Grenoble Alpes, Grenoble, France, 2017.
17. Delétang, T.; Barnel, N.; Franger, S.; Assaud, L. Transposition of a weighted Ah-throughput model to another Li-ion technology: Is the model still valid? New insights on the mechanisms. In Proceedings of the Coupled Problems Conference, Rhodes, Greece, 12–14 June 2017.
18. Dubarry, M.; Truchot, C.; Cugnet, M.; Liaw, B.Y.; Gering, K.; Sazhin, S.; Jamison, D.; Michelbacher, C. Evaluation of commercial lithium-ion cells based on composite positive electrode for plug-in hybrid electric vehicle applications. Part I: Initial Characterizations. *J. Power Source* **2011**, *196*, 10328–10335. [[CrossRef](#)]
19. Delacourt, C.; Kassem, M. Postmortem analysis of calendar-aged graphite LiFePO₄ cells. *J. Power Sources* **2013**, *235*, 159–171. [[CrossRef](#)]
20. De Hoog, J.; Timmermans, J.-M.; Ioan-Stroe, D.; Swierczynski, M.; Jaguemont, J.; Goutam, S.; Omar, N.; Van Mierlo, J.; Van den Boosche, P. Combined cycling and calendar capacity fade modelling of a NMC oxide cell with real-life profile validation. *Appl. Energy* **2017**, *200*, 47–61. [[CrossRef](#)]
21. Schmalstieg, J.; Käbitz, S.; Ecker, M.; Sauer, D.U. A holistic aging model for Li(NiMnCo)O₂ based 18650 lithium-ion batteries. *J. Power Sources* **2014**, *257*, 325–334. [[CrossRef](#)]
22. Dubarry, M.; Qin, N.; Brooker, P. Calendar aging of commercial Li-ion cells of different chemistries-A review. *Curr. Opin. Electrochem.* **2018**, *9*, 106–113. [[CrossRef](#)]
23. Berecibar, M.; Dubarry, M.; Omar, N.; Villarreal, I.; Van Mierlo, J. Degradation mechanism detection for NMC batteries based on Incremental Capacity curves. *World Electr. Veh. J.* **2016**, *8*, 350–361. [[CrossRef](#)]
24. Dubarry, M.; Devie, A.; Liaw, B.Y. The Value of Battery Diagnostics and Prognostics. *J. Energy Power Sources* **2014**, *1*, 242–249.
25. Weng, C.; Cui, Y. On-board state of health monitoring of lithium-ion batteries using incremental capacity analysis with support vector regression. *J. Power Sources* **2013**, *235*, 36–44. [[CrossRef](#)]
26. Li, Y.; Abdel-Monem, M.; Gopalakrishnan, R.; Berecibar, M.; Nanini-Maury, E.; Omar, N.; van den Bossche, P.; Van Mierlo, J. A quick on-line state of health estimation method for Li-ion battery with incremental capacity curves processed by Gaussian filter. *J. Power Sources* **2018**, *373*, 40–53. [[CrossRef](#)]
27. Riviere, E.; Venet, P.; Sari, A.; Meniere, F.; Bultel, Y. LiFePO₄ Battery State of Health Online Estimation Using Electric Vehicle Embedded Incremental Capacity Analysis. In Proceedings of the 2015 IEEE Vehicle Power and Propulsion Conference (VPPC), Montreal, QC, Canada, 19–22 October 2015.
28. Cabelguen, P.E. Analyse de la Microstructure des Matériaux Actifs D'électrode Positive de Batteries Lithium-Ion. Ph.D. Thesis, Université Grenoble Alpes, Grenoble, France, 2016.
29. Dubarry, M.; Truchot, C.; Liaw, B.Y. Cell degradation in commercial LiFePO₄ cells with high-power and high energy designs. *J. Power Source* **2014**, *258*, 408–419. [[CrossRef](#)]
30. Bloom, I.; Walker, L.K.; Basco, J.; Abraham, D.; Christoffersen, J.; Ho, C. Differential voltage analyses of high-power lithium cells 4. Cells containing NMC. *J. Power Sources* **2010**, *195*, 877–882. [[CrossRef](#)]
31. Dubarry, M.; Truchot, C.; Liaw, B.Y. Synthesize battery degradation modes via a diagnostic and prognostic model. *J. Power Sources* **2012**, *219*, 204–216. [[CrossRef](#)]
32. Dubarry, M.; Truchot, C.; Liaw, B.Y.; Gering, K.; Sazhin, S.; Jamison, D.; Michelbacher, C. Evaluation of commercial lithium-ion cells based on composite positive electrode for plug-in hybrid electric vehicle applications. Part II: Degradation mechanism under 2C cycle aging. *J. Power Source* **2011**, *196*, 10336–10343. [[CrossRef](#)]

33. Dubarry, M.; Svoboda, V.; Hwu, R.; Liaw, B.Y. Incremental Capacity Analysis and Close-to-Equilibrium OCV measurements to quantify capacity fade in commercial rechargeable lithium batteries. *Electrochem. Solid State Lett.* **2006**, *9*, A454–A457. [[CrossRef](#)]
34. Fongy, C.; Jouanneau, S.; Guyomrd, D.; Badot, J.C.; Lestriez, B. Electronic and Ionic Wirings Versus the Insertion Reaction Contributions to the Polarization in LiFePO₄ Composite Electrodes. *J. Electrochem. Soc.* **2010**, *157*, A1347–A1353. [[CrossRef](#)]
35. Bloom, I.; Jansen, A.N.; Abraham, D.P.; Knuth, J.; Jones, S.A.; Battaglia, V.S.; Henriksen, G.L. Differential voltage analyses of high-power lithium cells 1. Technique and application. *J. Power Sources* **2005**, *139*, 295–303. [[CrossRef](#)]
36. Bloom, I.; Christophersen, J.; Gering, K. Differential voltage analyses of high-power lithium cells 2. Applications. *J. Power Sources* **2005**, *139*, 304–313. [[CrossRef](#)]
37. Li, X.; Wang, Z.; Zhang, L.; Zou, C.; Dorrell, D. State-of-health estimation for Li-ion batteries by combining the incremental capacity analysis with grey relational analysis. *J. Power Sources* **2019**, *410–411*, 106–114. [[CrossRef](#)]
38. Buchberger, I.; Seidlmaier, S.; Pokharel, A.; Piana, M.; Hattendorff, J.; Kudejova, P.; Gilles, R.; Gasteiger, H.A. Aging analysis of Graphite/LiNiMnCoO₂ cells using XRD, PGAA, and AC Impedance. *J. Electrochem. Soc.* **2015**, *162*, 2737–2746. [[CrossRef](#)]
39. Stiaszny, B.; Ziegler, J.C.; Krauß, E.E.; Zhang, M.; Schmidt, J.P.; Ivers-Tiffée, E. Electrochemical characterization and post-mortem analysis of aged LiMn₂O₄—NMC/graphite lithium ion batteries part ii: Calendar aging. *J. Power Source* **2014**, *195*, 61–75. [[CrossRef](#)]
40. Ansean, D.; Dubarry, M.; Devie, A.; Liaw, B.Y. Operando lithium plating quantification and early detection of a commercial LiFePO₄ cell cycled under dynamic driving schedule. *J. Power Sources* **2017**, *356*, 36–46. [[CrossRef](#)]



© 2019 by the authors. Licensee MDPI, Basel, Switzerland. This article is an open access article distributed under the terms and conditions of the Creative Commons Attribution (CC BY) license (<http://creativecommons.org/licenses/by/4.0/>).